Influence of Fabrication Conditions on the Structural Characteristics and the Magnetic Properties of $FeAl_2O_4$

Takayuki Nakane[1], Satoshi Ishii[2], Tetsuo Uchikoshi[1] and Takashi Naka[1]

1. National Institute for Materials Science, Research Center for Functional Materials, 1-2-1, Sengen, Tsukuba, Ibaraki 305-0047, Japan

2. Tokyo Denki University, Department of Physics, Hatoyama, Hiki-gun, 350-0394 Saitama, Japan

Abstract

We report a systematic evaluation of the magnetic properties of $FeAl_2O_4$ focusing on the relationship between the fabrication conditions and its structural characteristics, in order to improve ceramics processing in applications of this material. For this purpose, the most important factor to control is the inversion parameter, expressed as y in the $(Fe_{1-y}Al_y)(Al_{1-y/2}Fe_{y/2})_2O_4$ composition, which is relatively high for the spinel aluminate of a transition metal. The magnetic properties of these samples all shows the spin glass phenomenon at low temperatures, and the cusp temperature depends systematically on this y value. This means that the evaluation of these magnetic properties will be an effective way to predict some characteristics of product $FeAl_2O_4$. Additionally, this study found an anomaly in the structural and magnetic characteristics of $FeAl_2O_4$ fabricated at a low temperature. This is thought to originate in a tiny and a small amount of impurity. It will be key for discussing the quality of chemically synthesized $FeAl_2O_4$, which is typically produced at low temperatures.

Introduction

There is no doubt that the crystal structure plays an important role in the investigation of functional ceramics. Following this concept, the spinel structure, with its isotropic cubic symmetry and flexible tuning of its chemical composition, is particularly attractive. The compositional formula of a spinel oxide is expressed as AB_2O_4, where *A* and *B* indicate di- and tri-valent metal cations, respectively. The cations that exist at each type of site (i.e. A^{2+} and B^{3+}) respectively form characteristic tetrahedral and octahedral structures with the coordinating anion (i.e. O^{2-}). The various attractive-properties found in spinel oxides mainly originate in the electronic states of these two metal cations. Consequently, site-exchange phenomenon between these two metal cations often becomes the substantive issue for discussing the properties of spinel oxides.[1,2] This phenomenon is so prevalent that the degree of site-exchange is often defined through inversion parameter, *y*, meaning the degree of distribution of A^{2+} in the *B* site, i.e. *y* of a $(A^{2+}{}_{1-y}B^{3+}{}_{y})(B^{3+}{}_{2-y}A^{2+}{}_{y})O_4$ composition. Differences in *y* values sometimes result in the markedly different properties of the spinel material, even though the chemical composition is often expressed simply as AB_2O_4 in many case[3]. This point is often the hidden reason for contradictions between experimental results reported by different groups. This *y* value should not be thought of as a parameter that can be neglected in the study of all spinel materials.

Application of spinel materials have been widely investigated in a wide range of scientific fields including magnetism[4,5], catalytic chemistry[6-9], optical science[10-12], pigments[13] and so on. In particular,

catalytic applications are meaningful and promising challenges. However, some issues can be imagined at the nascent stage for the roadmap to fully launch a catalytic application studies of the spinel materials., For instance, catalytic materials commonly requires effective chemical synthesis procedures for industrial application, since they should be produced at low cost. In addition, the processes should be applicable for the mass or large-scale production. For example, mass production is required for nanoparticle forms and large-scale production is required for the porous bulk forms used as a heterogeneous catalyst. The chemical synthesis of ceramic materials is usually performed at relatively low temperatures under 200 ^{o}C, and this tends to increase the inversion parameter in case of spinel materials.[14] Increasing the inversion parameter is generally thought of as a negative factor for the physical properties of the spinel materials. However, it is not a simple in case of the catalytic applications. Appropriate amount of the site exchange phenomenon is considered as one of the possibility of enhancing the catalytic performance in case of transition metal aluminates expressed as $M\mathrm{Al_2O_4}$ (*M*: transition metal), since it increases the amount of Al^{3+} in tetrahedral coordination.[15,16] That is, chemical synthesis of spinel material should control the inversion parameter precisely. In this case, an effective evaluation method is also required in order to accurately measure this quantity.

Recently, Braga et al reported the attractive potential of hercynite ($\mathrm{FeAl_2O_4}$) for application as a chemical synthesis catalyst to produce styrene, one of the important chemical component in the modern worldwide.[17,18] An important consideration is that $\mathrm{FeAl_2O_4}$ consist of the ubiquitous elements, rather than

expensive metals such as rhodium or platinum. Also, the chemical industry has recently faced a drastic paradigm shift in fabrication processes brought about by the change of natural resources for these components from naphtha to methane hydrate. These considerations encourage us to further investigate the potential of $FeAl_2O_4$ as a synthesis catalyst of chemical components like styrene from new feedstocks.

There is a long history of the study of transition metal aluminates with the composition of MAl_2O_4 but we have found few fabrications that discuss $FeAl_2O_4$.[17-19] There are probably two main reasons for this lack. One is that attractive applications for this oxide had not been discovered before the report by Braga et al.[17] The second is that the fabrication of $FeAl_2O_4$ is relatively difficult compared to other metal spinel aluminates, since it requires preventing the oxidation of Fe^{2+}.[19] Unfortunately, the synthesis conditions used for spinel aluminates easily oxidize Fe^{2+} to Fe^{3+}, so this point will probably be a future issue in investigating the catalytic performance of $FeAl_2O_4$. There are few reports on the relationship between the precise structure and the physical properties of $FeAl_2O_4$. In particular, the influence of the fabrication conditions on the inversion parameter and the resulting physical properties have not yet been clarified for $FeAl_2O_4$.

Given this background, we planned to obtain systematic data about the relationship between the fabrication conditions and the precise structure of $FeAl_2O_4$ as the first step for starting its study of its application. Here, we focus on the inversion parameter of the products as the most important structural parameter. Additionally, the magnetic properties of all the samples were also evaluated, since they often give us a meaningful principle to understand the usefulness of the product in the case of the processing

studies of the materials including magnetic elements.

Experimental

The $FeAl_2O_4$ samples were prepared as polycrystalline powders. The starting materials of FeO (Kojundo chemical Laboratory: 99.5 %) and γ-Al_2O_3 (STREM chemicals: min 97 %) were mixed at the nominal ratio of 1:2 and pelletized. The pelletized mixture was placed in an alumina crucible (99.9%) and encapsulated in a quartz tube under vacuum atmosphere and set in a furnace. This tube was heated up to the sintering temperature for 3 hours, kept at that temperature for 24 hours and cooled down to 200 ^oC slowly. The sintering temperature was 900 ^oC or 1100 ^oC or 1200 ^oC. On the other hand, the cooling time was controlled in the range between quenching directly from the furnace ($\approx$ 0 hour) and 200 hours. This manuscript labels all samples with the fabrication conditions in the style of *Temp_time*, i.e. *Temp* and *time* are the sintering temperature and the cooling time from *Temp* to 200 ^oC, respectively. For instance, the sample labeled 1200_40 is the powder sintered at 1200 ^oC for 24 h and cooled from this temperature to 200 ^oC for 40 hours (25 ^oC/h).

The product $FeAl_2O_4$ samples were evaluated by X-ray diffraction (XRD, Mini-FLEX: Rigaku) measurements using Cu Kα (l = 1.542 Å) radiation. In addition, the structural information of these samples are analyzed from the Synchrotron XRD (SXRD) patterns obtained at the SPring-8 (BL15XU) beamline at Harima in Japan.[20,21] The powder diffractometer using X-ray beam with λ = 0.65298 Å (Nb K

edge Bearden) was used by scanning in steps of 0.003 degree over the 2θ range of 5 ~ 80 degree. Samples packed in the capillary tube with a diameter of 0.2 mm was used for the measurements and the data were collected at room temperature. The measured SXRD data were all refined by the Rietveld method[22] using the RIETAN-FP software.[23] The structural model was cubic with the space group of *F*d-3m (No. 227-2). The total occupancies of Fe^{2+} and Al^{3+} at the *A* site and Al^{3+} and Fe^{2+} at the *B* site were both fixed at 1.0, and the total amount of Fe^{2+} and Al^{3+} was also restricted in order to express the composition to be $(Fe_{1-y}Al_y)(Al_{1-y/2}Fe_{y/2})_2O_4$. The coordinate values of *A* and *B* sites are (0.125, 0.125, 0.125) and (0.5, 0.5, 0.5) for our Rietveld refinement, respectively, thus the refined characteristic structural parameters, except for some functional parameters, are basically the lattice constant, *a*, and *u* of the oxygen site (*u*, *u*, *u*). It means that our Rietveld refinement is a quite simple analysis. Fourier transform infrared (FT-IR, FT/IR-6200: JASCO) spectra performed on samples in KBr pellets provided useful confirmatory evidence of structural changes.

The magnetic properties of the products were evaluated by using a superconducting quantum interference device magnetometer (SQUID, MPMS-XL: Quantum Design). Firstly, the temperature dependence of the magnetic susceptibilities, χ_{DC}, was measured at 10 kOe DC magnetic fields. The Weiss temperature, Θ, and the Curie constant for 1 mol amount, C_{mol}, were calculated from the experimental data of each temperature, *T*, between 120 and 300 K using the Curie−Weiss (CW) law, $\chi_{mol} = C_{mol}/(T-\Theta)$. The effective moment, p_{eff}, was calculated as the equation, $p_{eff}\,\mu_B = \sqrt{3k_BC_{mol}/N_A}$, where k_B, N_A, and μ_B are the

Boltzmann constant, Avogadro number and Bohr magneton, respectively. On the other hand, the theoretical effective moment, $p_{\text{eff-cal}}$ can be calculated with the equation, $p_{\text{eff-cal}} = g\sqrt{s(s+1)}$, where g and s are the g-factor and spin quantum number of the magnetic element, respectively. Thus, if we regard $p_{\text{eff}} = p_{\text{eff-cal}}$ and fix $s = 4/2$ as the value for Fe^{2+}, the g-factor of the samples are calculated from the obtained C_{mol}.[8,24]

Furthermore, this study tried to check the temperature dependence of the AC susceptibilities, χ_{AC}, with the magnitude of 5 Oe for some samples in order to see the frequency dependence in the range between 15 and 1500 Hz.

Structural Characteristics

Figure 1 (a) shows the XRD patterns of all product samples. They are judged to be single phase $FeAl_2O_4$ spinel, although high resolution SXRD measurement detected very small amount of Al_2O_3 peaks as the prime impurity for the samples sintered at 900 ^{o}C (see Figure 1 (b)). The intensity of the Al_2O_3 peaks are quite small, hence we ignored them in all structural analysis in this study. On the other hand, this information about Al_2O_3 peaks indicates the existence of a very small amount of iron-rich regions or phase in the sample that may has possibility affect the magnetic properties.

Table 1 summarizes the main results of the Rietveld refinement for the SXRD results of all samples. Here, R_{wp} and S indicates the reliability value of weighted pattern and goodness of the fitting, respectively. These data were easily refined, and thus the values of the reliability indicators were good. We found that

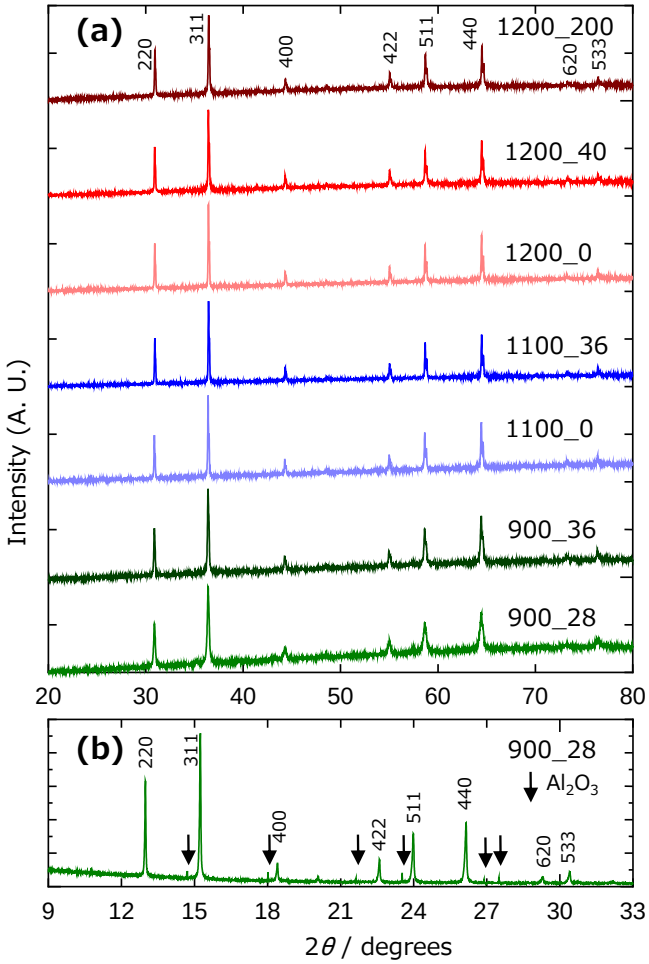

Figure 1 (a) XRD patterns of product $FeAl_2O_4$ samples. (b) SXRD patterns pf 900_28.

the inversion parameters were relatively all higher than that of other spinel aluminates like $CoAl_2O_4$.[8] It is one of the unique characteristics of the $FeAl_2O_4$ system. Figure 2 plots the lattice constant against inversion parameter of our samples. The data looks scattered, but it does show as general trend.[25-27] That is, both increasing the heating temperature and slowing the cooling rate contribute to reduce the inversion parameter of the spinel oxide. This trend is also roughly seen in the result of FT-IR measurements (see Figure 3). Here, an increase in the inversion parameter relatively enhances the intensity of the peak shoulder around 750

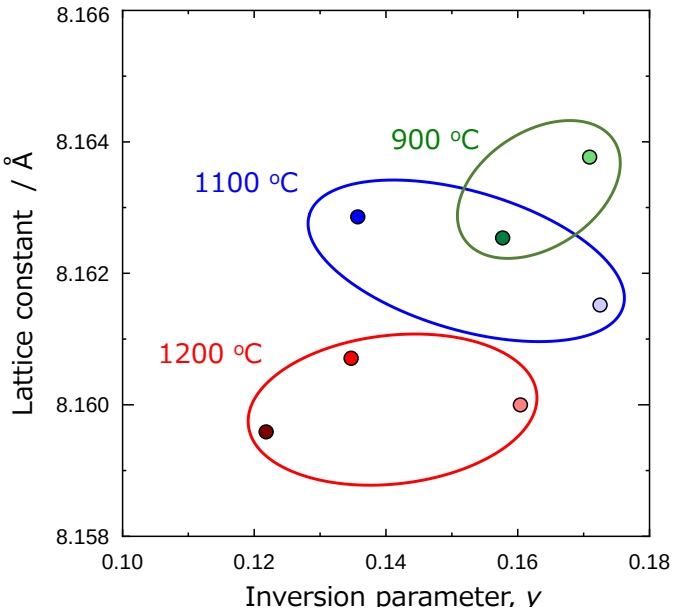

Figure 2 Relationship between the inversion parameter and the lattice constant of product $FeAl_2O_4$ samples. The plotted color of each sample corresponds to that in Figure 1. The square symbol (■) indicates the quenched sample. The other symbols indicate the rate of cooling as a circle (● : 25 °C/h), an inverted triangle (▼ : 19.4 °C/h) and a triangle (▲ : 5 °C/h) , respectively.

cm^{-1} and decreases the peak intensity around 520 cm^{-1} (see the arrowed shoulder and peak in the figure). These changes are considered to be strongly influenced by the site exchange phenomenon.[28] The inversion parameter is commonly believed to be the most closely connected factor that determines the lattice parameter of a spinel oxide. However, Figure 2 shows that the lattice constant depends on the heating temperature rather than the inversion parameter. As the reason, we considered as follows. At first, slowing the cooling rate apparently reduces the inversion parameter. On the other hand, high temperature sintering is generally thought to enhance the homogenization of the cation distribution.[29] Hence, the heating temperature is not considered to be the critical parameter to reduce the inversion parameter. However, higher heating temperature results in the elongation of the cooling time. It is thought to promote the

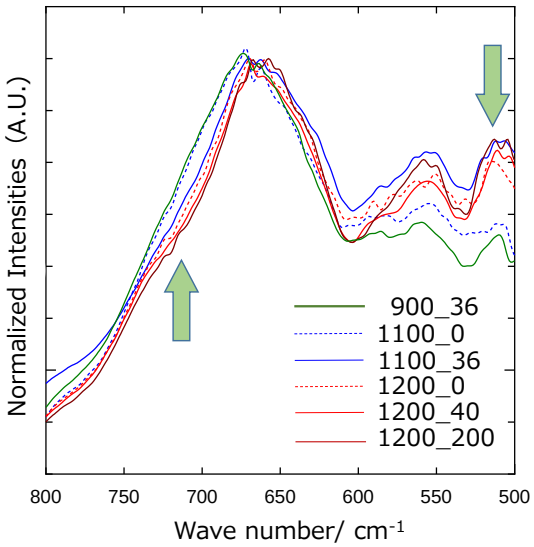

Figure 3 FT-IR spectra normalized by the highest peak in the band around 675 cm^{-1} of product $FeAl_2O_4$ samples. The plotted color of each sample corresponds to that in Figure 1.

appropriate ordering of cations (i.e. reducing the inversion parameter). In fact, the inversion parameter appears to be similar between 1200_40 and 1100_36 (in both cases the cooling rate is 25 °C/h) and between 1200_0 and 1100_0. Probably, the homogeneity of the overall cation distribution was more important for reducing the lattice constant than reducing the inversion parameter.

Table 1 Experimental results of product $FeAl_2O_4$ samples with respect to the refined structure and magnetic characteristics

	1200_200	1200_40	1200_0	1100_36	1100_0	900_36	900_28
a (Å)	8.15958(1)	8.16070(2)	8.15999(1)	8.16285(2)	8.16151(1)	8.16253(3)	8.16376(6)
u	0.26399(4)	0.26377(6)	0.26387(4)	0.26381(5)	0.26354(4)	0.26382(5)	0.26375(7)
y	0.1220(14)	0.1348(16)	0.1606(12)	0.1358(14)	0.1726(10)	0.1578(14)	0.1710(20)
R_{wp}	4.160	4.016	3.118	2.816	2.500	2.907	3.508
S	2.893	2.636	2.011	1.768	1.585	1.839	2.21
C_{mol} (emu K/Oe)	3.80	3.93	3.85	3.90	3.92	4.47	7.07
p_{eff}	5.51	5.60	5.54	5.55	5.59	5.96	7.53
g	2.25	2.29	2.26	2.28	2.28	2.44	3.07
Θ (K)	-124.5	-128.9	-132.1	-134.0	-138.9	-164.8	-265.1
T_g (K)	11.4	12.5	12.2	13.2	13.4	15.2	39.5

Magnetic Properties

Figure 4 plots the reciprocal χ_{DC} of 1200_200 as a function of the temperature. This figure shows the typical curvature of $1/\chi_{DC}$-T plot for all samples. The data of high temperature region over 120 K can be easily fitted by the CW law (see the red line drawn in this figure). The C_{mol} (emu K/Oe), p_{eff}, g and Θ (K) values analyzed by this fitting procedures are also summarized in Table 1. Figure 5 plots the g values of samples against the inversion parameter. If we ignore the data of 900_36 and 900_28 from the discussion, thr site-exchange phenomenon looks to slightly increase the g value of Fe^{2+} (as in the dashed line drawn in Figure 5) within the margin of the analysis error. The systematic change of g value influenced by the y value

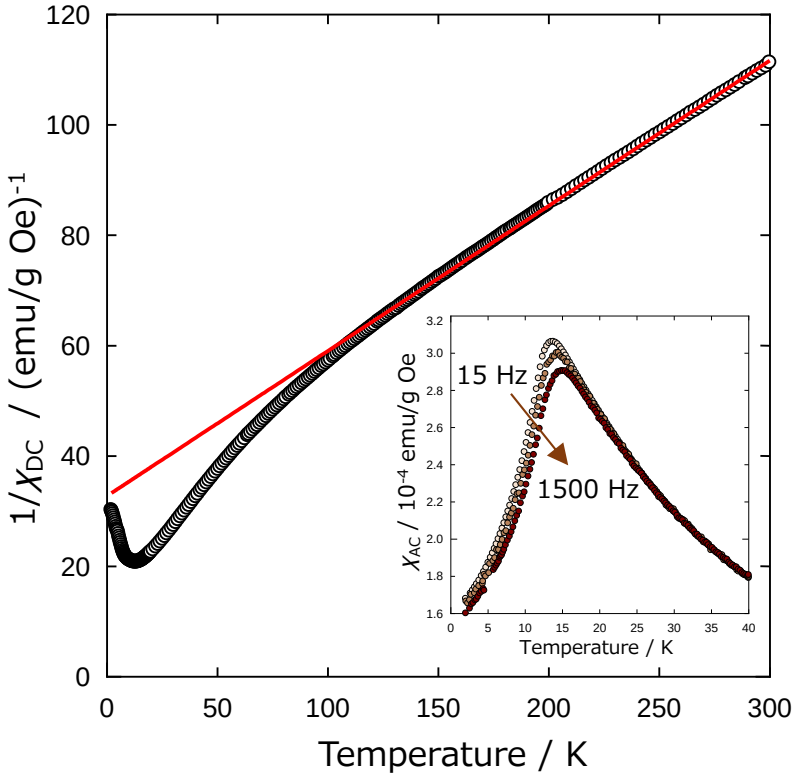

Figure 4 Temperature dependence of the reciprocal χ_{DC} measured for 1200_200 as a typical $1/\chi_{DC}$-T curve of product $FeAl_2O_4$ samples. The insert shows the frequency dependence of the χ_{AC}-T curve of the same sample.

indicated by this line is quite similar to the data for some other spinel aluminate series (MAl$_2$O$_4$),[30-33] and is basically caused by the difference in the coordination of Fe^{2+} between tetrahedral (A site) and octahedral (B site). Because, the B site of the spinel structure tend to require the trivalent cation,[34] its appearance is also supposed to be the reason for the changes of g value. In fact, the p_{eff} of Fe^{2+} is in the range of 5.2 ~ 5.5 in general, but our all calculated data show a slightly higher value.

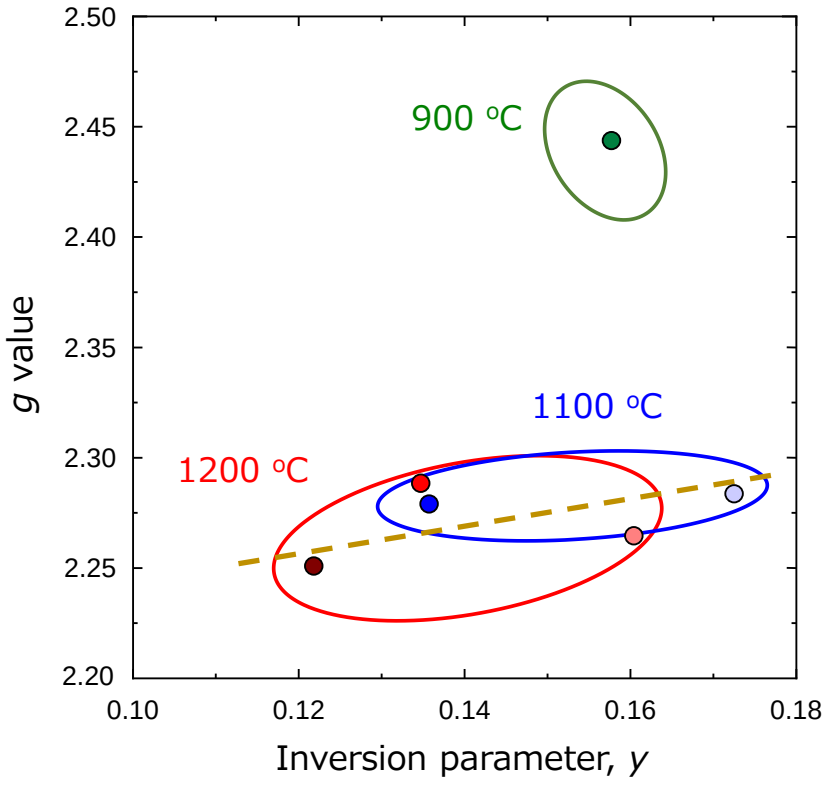

Figure 5 Calculated g values of product FeAl$_2$O$_4$ samples plotted against the inversion parameter. The plotted color of each sample corresponds to that in Figure 1. Plotted symbols are distinguished by the cooling speed of the sample as a square (■: quenched), a circle (●: 25 °C/h), an inverted triangle (▼: 19.4 °C/h) and a triangle (▲: 5 °C/h), respectively.

On the other hand, it is difficult to explain the exceptionally large value of p_{eff} and g values of 900_36 and 900_28. This abnormally deviated data presumably is caused by the existence of another type of

anomaly in these samples. The site-exchange phenomenon itself is not considered to form some kind of long-range spin ordering in the spinel structure. Also, the *y* values of 900_36 and 900_28 do not seem to be enough large to form such ordering. Therefore, we speculate that these exceptionally large *g* values imply the localization of Fe^{2+} and/or Fe^{3+} in the spinel oxide. The discussions in the next section also support this speculation.

As the next step, we should discuss the $1/\chi_{DC}$-*T* plot in Figure 4 in the low temperature region under 120 K. The experimental data departs from the CW law, and we can see the cusp at around 12 K. The inset figure shows the frequency dependence of this cusp observed for the χ_{AC}-*T* plot of the same sample (1200_200). This cusp is considered to originate in the spin glass phenomenon, since it is often reported for some spinel aluminates including a 3*d*-transition-metal element as the *A* site cation.[30-33] The inset shows that enhancing the frequency of the applied AC field increases the cusp temperature and decreases the magnitude of the susceptibility peak. These trends are reasonable to understand it as the cusp symbolizing the spin glass phenomenon. Note that, these cusp temperatures, T_g, are slightly higher than that of other spinel aluminates like $CoAl_2O_4$.[10] This is considered to be due to the relatively higher inversion parameter of $FeAl_2O_4$ samples. The magnetic behaviour of $FeAl_2O_4$ is considered to be antiferromagnetism in the low temperature region in case of a sample not subject to the without site-exchange phenomenon (i.e. $y = 0$).[35] However, preparing antiferromagnetic $FeAl_2O_4$ without site-exchange is quite difficult. In practice, the magnetic ordering among the *A* site Fe^{2+} ions is randomly disrupted by non-magnetic Al^{3+} by the site-

exchange phenomenon. The magnetic ordering of the *A* site cation in this case has been actively discussed for some MAl$_2$O$_4$ series recently from the physics viewpoint.[36-40] Here, we should not restrict the magnetic ordering via the exchange interaction only between nearest neighbors of M^{2+} at the *A* site, but we should additionally take into account the influence of the next nearest neighbor cations. Thus, the magnetic ordering of Fe^{2+} becomes quite complicate when some disorder like site-exchange phenomenon is introduced. Furthermore, the magnetic moment of Fe^{2+} at the *B* site is also considered to be a non-isolated state. The distance between a Fe^{2+} at the *A* site and one at the *B* site is shorter than that to the *A* site one of the next nearest neighbors. The *y* values of our samples were all larger than 0.125 (= 2/16), and the number of *B* site cations is 16 in the unit cell of spinel structure. In that case, there is the possibility to form rectangular bonding between two Fe^{2+} and O^{2-} in the unit cell. This rectangular bonding pattern has the potential to form a different magnetic ordering from the antiferromagnetism of *A* site according to the Kanamori-Goodenough rule.[41-43] These complexities in the magnetic ordering of Fe^{2+} are considered to give rise to the strong magnetic frustration for the long range spin-ordering of $FeAl_2O_4$. This scenario is the considered as the reason for the spin glass phenomenon to appear as the overall magnetism of $FeAl_2O_4$ in the temperature region.[33] In that case, the T_g should correspond to the inversion parameter systematically. Table 1 includes the T_g values for all our samples, and Figure 6 plots these T_g against the *y* values. The trend that increasing the *y* value results in enhancing the T_g of $FeAl_2O_4$ can been seen from Figure 6. If we ignore the data of 900_36 and 900_28 from the discussion (see the dashed line in the figure), this trend is quite

consistent with the discussion about the *g* value. Hence, we concluded that the site-exchange phenomenon essentially increases T_g of the $FeAl_2O_4$ system as seen in the dashed line in Figure 6. This figure also plots the $|\Theta|$ using the values in Table 1 with the 10 times larger scale of T_g. These plots are good agreement for all samples except for 900_28. The difference between T_g and Θ is often regarded as an indicator of the magnetic frustration in discussions of the spin glass materials.[30,44] From this viewpoint, the 10 times scale is enough to judge the existence of the magnetic frustration. This result also supports our explanation about the spin glass phenomenon observed for our $FeAl_2O_4$.

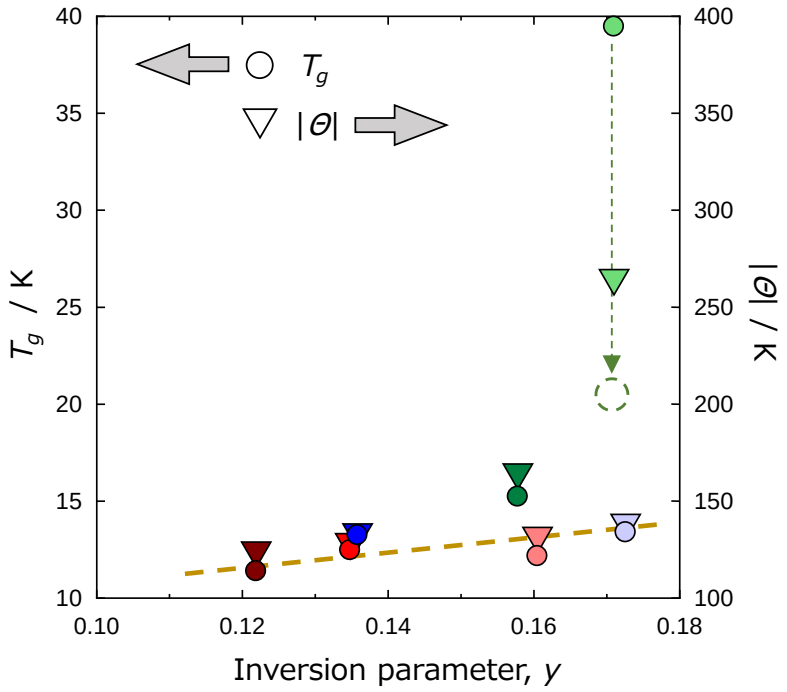

Figure 6 Relationship between the inversion parameter and the cusp temperature, T_g, (filled symbols plotted on the left y-axis scale) and the absolute values of the Weiss temperature, $|\Theta|$, (cross mark, ×, plotted on the right y-axis scale) of product $FeAl_2O_4$ samples. Plotted symbols of T_g are distinguished by the cooling speed of the sample as a square (■: quenched), a circle (●: 25 °C/h), a inverted triangle (▼: 19.4 °C/h) and a triangle (▲: 5 °C/h), respectively. The plotted color of each sample corresponds to that in Figure 1.

Discussion for the anomaly in $FeAl_2O_4$ sintered at 900 °C

This study succeeded in showing systematic trends with respect to the relationship between the structural characteristics and the magnetic properties in $FeAl_2O_4$ with the exceptions of the experimental data of 900_36 and 900_28 which were drastically different from our expectations.

Figure 7 compares the χ_{DC}-T curves of 1200_200 and 900_28. The cusp of 900_28 is apparently broader than that of 1200_200, and its magnitude is also higher. In addition, the χ_{DC}-T curve of 900_28 drastically changed with the value of the applied magnetic field (see the figure insert). This field dependence of 900_28 is apparently larger than that of the other our samples, and at first sight, looks as though it might be originating in superparamagnetism rather than the spin glass phenomenon. Proceeding from this viewpoint, we found a shoulder peak at around 20 K for the χ_{DC}-T curve of 900_28 at 0.1 kOe (see the insert in Figure 7). This shoulder peak was prominently observed only for 900_28. The T_g in Table 1 was determined from the main peak with the same criteria. However, the shoulder observed at around 20 K of 900_28 is probably the effective T_g originating in the site exchange phenomenon. This speculation is moreover consistent with the value of $|\Theta|$ discussed in Figure 6. If we regard the T_g of 900_28 as 20 K plotted as the dashed circle with a dashed arrow in Figure 6, the general trend between T_g , $|\Theta|$ and y seems to be more reasonable for our samples. In other words, the origin of the magnetic anomaly of 900_28 is considered to relate to the main peak of the χ_{DC}-T curve measured at 0.1 kOe. Then, the drastic shift

produced by increasing the applying magnetic-field and the broader shape of this main peak are considered to be the blocking temperature of the superparamagnetism signal. Therefore, the origin of the magnetic anomaly of 900_28 is considered to relate to the influence of superparamagnetism signal.

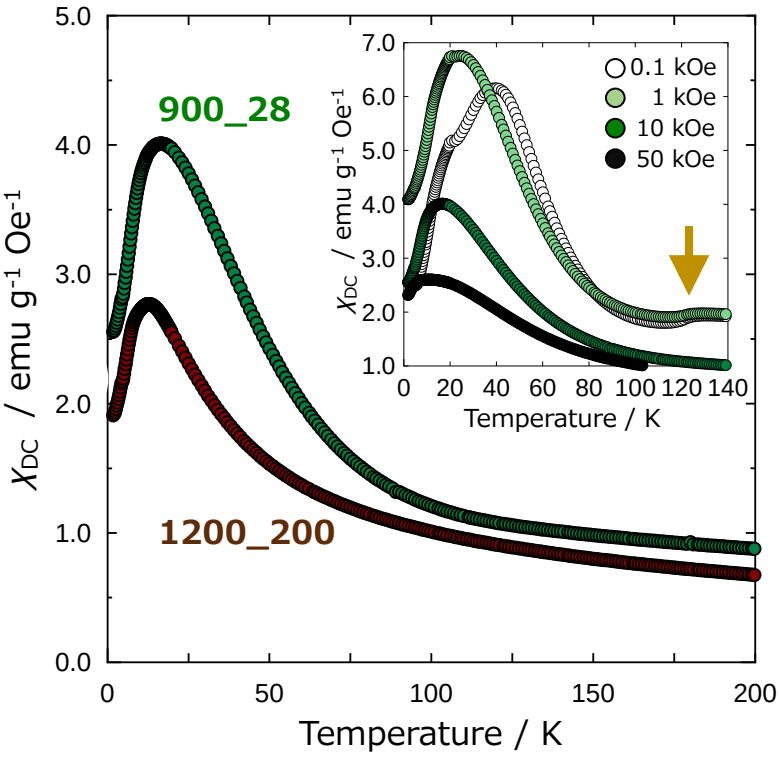

Figure 7 Dependence of the DC susceptibility at 10 kOe on the temperature for the zero field cooled measurement. The data are plotted for 1200_200 (brown circle) and 900_28 (green circle). The insert shows the field dependence of the χ_{DC}-T curve for 900_28.

The origin of this ferromagnetic signal is quite difficult to ascertain in principle, although several workers have reported on the ferromagnetism of $FeAl_2O_4$.[45-47] If the y of 900_28 is very high value, the ferromagnetic signal in this sample can be explained as the influence of Fe^{2+} at the B site. However, the y is not considered to be high enough for producing ferromagnetism. In addition, we found a tiny amount of

impurity Al_2O_3 from the SXRD peak. Therefore, we considered the possibility that a small amount of Fe_3O_4 is the origin of the ferromagnetism in our sample. In fact, we can identify a small kink around 120 K in the χ_{DC}-T curves of 900_28 at 0.1 kOe and 1 kOe (see the arrow of the insert in Figure 7), that is speculated to be the Verway transition[48,49]. The amount of Fe_3O_4 must be small, since the kink is not visible in the data measured at high magnetic fields. This consideration is supported by the SXRD patterns of 900_28 (see Figure 8), which are prominentlt asymmetric. These asymmetric peaks are speculated to imply the existence of a different phase with a similar lattice. Therefore, we concluded that the origin of the magnetic anomalies of 900_28 and 900_36 are the influence of a superparamagnetism signal caused by a small amount of Fe_3O_4 impurity.

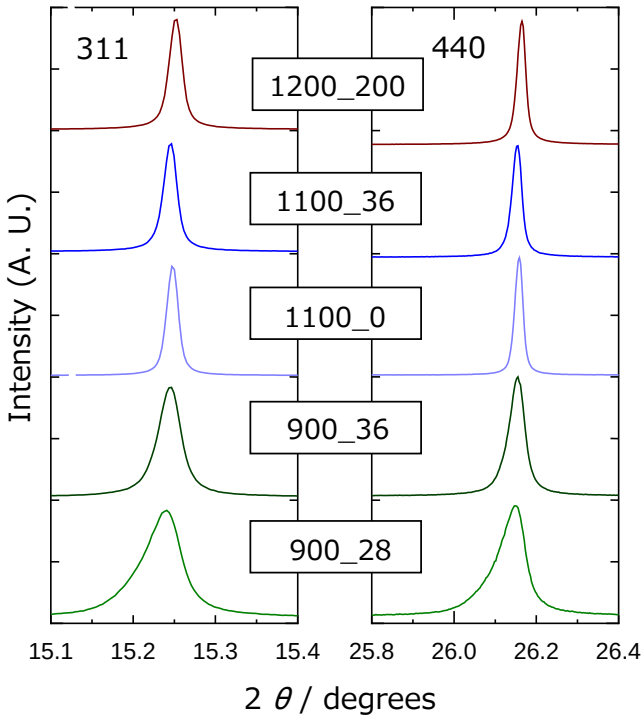

Figure 8 Deatil of SXRD peaks of some $FeAl_2O_4$ samples in this study. The plotted color of each sample corresponds to that in Figure 1.

Small differences in the fabrication conditions have the potential to change the homogeneity of the sample. Iron oxide, especially, has various stable phases corresponding to small changes in the fabrication conditions. Their importance is already recognized by most scientists, but this study indicates the necessity of further strict discrimination. For instance, the preparation conditions of 900_28 and 900_36 are quite similar, the difference being only the cooling rates of 25 ^{o}C/hour and 19 ^{o}C/hour respectively. This difference tends to be regarded as the "(almost the) same". However the magnetism of these two samples were quite different. According to the Figure 1 (XRD data of the solid state reaction), we tended to think that 900 ^{o}C is sufficiently high for to obtain a single phase of $FeAl_2O_4$. However, low temperature synthesis causes high inversion and involves the small amounts of impurities like Fe_3O_4, which can strongly influence the magnetism data. Probably, this point will be key for discussing the quality of chemically synthesized $FeAl_2O_4$, since it is basically fabricated at low temperatures.

Summary

The spinel $FeAl_2O_4$ has potential to be a synthesis catalyst for some valuable chemical component. However, there are few studies reporting on the relationship between the precise structure and the physical properties of this material. In particular, the influence of the fabrication conditions on the inversion parameter and its link to physical properties is yet unclear, a situation which promoted a systematic evaluation of this relationship.

Fabricated $FeAl_2O_4$ samples were essentially single phase, so that the structural analysis was straightforward. These experimental results reveals that the inversion parameter, y, of $(Fe_{1-y}Al_y)(Al_{1-y/2}Fe_{y/2})_2O_4$ is lowered by increasing the sintering temperature and lengthening the cooling time. However, the absolute inversion parameter values were relatively higher than that of other spinel aluminates, which leads to magnetic frustration of the overall magnetism of $(Fe_{1-y}Al_y)(Al_{1-y/2}Fe_{y/2})_2O_4$. Therefore, our all $FeAl_2O_4$ samples showed the spin glass phenomenon in the low temperature region of the χ_{DC}-T curve, and characteristics magnetic values obtained from this curve, i.e. C_{mol}, p_{eff}, g, Θ and T_g, were all dependent on the y of $(Fe_{1-y}Al_y)(Al_{1-y/2}Fe_{y/2})_2O_4$. In particular, T_g is consistently linked to the y value, and it corresponds to 1/10 of the $|\Theta|$ value. This appears to be universal for all samples sintered above 1100 ^oC. Consequently, the evaluation of these magnetic characteristics values will be an effective guidelines to judge the quality of synthesized $FeAl_2O_4$ as a chemical catalyst. This result is believed to be meaningful for the future investigation of $FeAl_2O_4$ for applying it as the catalyst.

On the other hand, this study found structural and magnetic abnormalities in the data for $FeAl_2O_4$ fabricated at 900 ^oC. They appear to originate in the existence of a tiny and a small amount of Fe_3O_4 or related impurity. The effects of small amounts of impurities will be an important consideration when discussing the quality of chemically synthesized $FeAl_2O_4$, which is usually fabricated at a low temperature.

Acknowledgements

This work was partially supported by a Grant-in-Aid for Challenging Exploratory Research, KAKENHI(16K13999).

References

[1] O'neill H S C. Temperature dependence of the cation distribution in $CoAl_2O_4$ spinel. Eur. J. Mineral. 1994;6:603-609.

[2] Nakatsuka A, Ikeda Y, Yamasaki Y, Nakayama N, Mizota T. Cation distribution and bond lengths in $CoAl_2O_4$ spinel. Solid State Commun. 2003;128:85-90.

[3] Tielens F, Calatayud M, Franco R, Recio J M, Pérez-Ramírez J, Minot C. J. Phys. Chem. B. 2006;110: 988-995.

[4] Hagiwara M, Kimura S, Nishihagi N, Suzuki T, Nohara M, Takagi H, Kindo K. High Field Magnetism of the Spinel Oxide $CoAl_2O_4$. J. Low Temp. Phys. 2010;159: 11-14.

[5] Maljuk A, Tsurkan V, Zestrea V, Zaharko O, Cervellino A, Loidl A, Argyriou D N. Floating-zone growth of large high-quality $CoAl_2O_4$ single crystals. J. Cryst. Growth, 2009; 311:3997–4000.

[6] Ji L, Tang S, Zeng H C, Lin J, Tan K L. CO_2 reforming of methane to synthesis gas over sol–gel-made Co/g-Al_2O_3 catalysts from organometallic precursors. Appl. Catalysis A. 2001;207:247-255.

[7] Walsh A, Yan Y, Al-Jassim M M, Wei S-H. Electronic, Energetic, and Chemical Effects of Intrinsic Defects and Fe-Doping of $CoAl_2O_4$: A DFT+*U* Study. J. Phys. Chem. C, 2008;112:12044-12050.

[8] Ahn K-S, Yan Y, Kang M-S, Kim J-Y, Shet S, Wang H, Turner J, Al-Jassim M M. $CoAl_2O_4$-Fe_2O_3 p-n nanocomposite electrodes for photoelectrochemical cells. *Appl*. *Phys*. *Lett*., 2009, 95, 022116/1-3.

[9] Ishii S, Nakane T, Furusawa T, Naka T. Influence of pH tuning at the precursor preparation process on the structural characteristics and catalytic performance of hydrothermally synthesized $ZnAl_2O_4$ nanoparticles. J. Asian Ceram. Soc. 2018;6:7-12.

[10] Nakane T, Naka T, Sato K, Taguchi M, Nakayama M, Mitsui T, Matsushita A, Chikyow T. Dalton Trans. Spectroscopic and crystallographic anomalies of $(Co_{1-x}Zn_x)Al_2O_4$ spinel oxide. **44**, 997-1008 (2015).

[11] Chen X Y, Ma C, Zhang Z J, Wang B N. Ultrafine gahnite ($ZnAl_2O_4$) nanocrystals: Hydrothermal synthesis and photoluminescent properties. Mater. Sci. Eng. B. 2008;151: 224-230.

[12] Miron I, Enache C, Vasile M, Grozescu I. Optical properties of $ZnAl_2O_4$ nanomaterials obtained by the hydrothermal method. Physica Scripta. 2012;T149:014064.

[13] Kock L D, De Waal D. Raman studies of the underglaze blue pigment on ceramic artefacts of the Ming dynasty and of unknown origins. J. Raman Spect. 2007;38:1480−1487.

[14] Ishii S, Nakane T, Furusawa T, Naka T. Synthesis of single-phase $ZnAl_2O_4$ nanoparticles via a wet chemical approach and evaluation of crystal structure characteristics. Cryst. Res. Technol. 2016;51:324–332.

[15] Knözinger H, Ratnasamy, P. Catalytic Aluminas: Surface Models and Characterization of Surface Sites.

Catal. Rev. 1978;17;31-70.

[16] Zecchina A, Coluccia S, Morterra C. Infrared Sectra of Molecules Adsorbed on Oxide durfaces. Appl. Spectrosc. Rev. 1985;21;259-310.

[17] Braga T P, Longhinotti E, Pinheiro A N, Valentini A. Synthesis of hybrid spheres for the dehydrogenation of ethylbenzene in the presence of CO_2. Appl. Catal. A: Gen. 2009;362:139–146.

[18] Batista A H de M, Ramos F S O, Braga T P, Lima C L, Sousa F F de, Barros E B D, Filho J M, Oliveira A S de, Sousa J R de, Valentini A, Oliveira A C. Mesoporous MAl_2O_4 (M= Cu, Ni, Fe or Mg) spinels: Characterisation and application in the catalytic dehydrogenation of ethylbenzene in the presence of CO_2. Appl. Catal. A: Gen. 2010; 382: 148-157.

[19] Chen J, Yu L, Sun J, Li Y, Xue W. Synthesis of hercynite by reaction sintering. J. Euro. Ceram. Soc. 2011;31:259-263.

[20] Tanaka M, Katsuya Y, Yamamoto A. A new large radius imaging plate camera for high-resolution and high-throughput synchrotron x-ray powder diffraction by multiexposure method. Rev. Sci. Instrum. 2008;79:075106.

[21] Tanaka M, Katsuya Y, Matsushita Y, Sakata O. Development of a synchrotron powder diffractometer with a one-dimensional X-ray detector for analysis of advanced material. J. Ceram. Soc. Jpn. 2013;121:287-290.

[22] Rietveld H M. A profile refinement method for nuclear and magnetic structures. J. Appl. Cryst.

1969;2:65-71.

[23] Izumi F, Momma K. Three-dimensional visualization in powder diffraction. Sol. Stat. Phenom. 2007;130:15-20.

[24] Naka T, Sato K, Matsushita Y, Terada N, Ishii S, Nakane T, Taguchi M, Nakayama M, Hashishin T, Ohara S, Takami S, Matsushita A. Multistage ordering and critical singularities in $Co_{1-x}Zn_xAl_2O_4$ ($0 \leq x \leq 1$): Dilution and pressure effects in a magnetically frustrated system. Phys. Rev. B. 2015;91:224412.

[25] Larsson L, O'Neill H St C, Annersten H. Crystal chemistry of synthetic hercynite ($FeAl_2O_4$) from XRD structural refinements and Moessbauer spectroscopy. Eur. J. Mineral. 1994;6:39-51.

[26] Peterson R C, Lager G A, Hitterman R L. A time-of-flight neutron powder diffraction study of $MgAl_2O_4$ at temperatures up to 1273 K. Am. Mineral. 1991;76:1455–1458.

[27] Shishin D, Prostakova V, Jak E, Decterov S A. Critical assessment and thermodynamic modeling of the Al–Fe–O system. Metall. Mater. Trans. B. 2016;47:397-424.

[28] Tatarchuk T, Shyichuk A, Lamkiewicz J,Kowalik J. Inversion degree, morphology and colorimetric parameters of cobalt aluminate nanopigments depending on reductant type in solution combustion synthesis. Ceram. Int. 2020;46:14674-14685.

[29] Harrison R J, Redfern S A T, O'Neill H St C. The temperature dependence of the cation distribution in synthetic hercynite ($FeAl_2O_4$) from in-situ neutron structure refinements. Am. Mineral.

1998;83:1092–1099.

[30] Tristan N, Hemberger J, Krimmel A, Krug von Nidda H A, Tsurkan V, Loidl A. Geometric frustration in the cubic spinel MAl$_2$O$_4$ (M = Co, Fe, and Mn). Phys. Rev. B. 2005;72:174404.

[31] Dutta D P, Sharma G. Synthesis and magnetic behavior of spinel $FeAl_2O_4$ nanoparticles. Mater. Sci. Eng. B. 2011;176:177-180.

[32] Hanashima K, Kodama Y, Akahoshi D, Kanadani C, Saito T. Spin Glass Order by Antisite Disorder in the Highly Frustrated Spinel Oxide $CoAl_2O_4$. J. Phys. Soc. Jpn. 2013;82:024702.

[33] Nair H S, Kumar K R, Strydom A M. Spin freezing in the spin-liquid compound $FeAl_2O_4$. Phys. Rev. B 2015;91: 054423.

[34] Jastrzębska I, Szczerba J, Stoch P, Błachowski A, Ruebenbauer K, Prorok R, Śnieżek E. Crystal structure and Mössbauer study of $FeAl_2O_4$. NUKLEONIKA. 2015;60:47-49.

[35] Roth W L. Magnetic properties of normal spinels with only a-a interactions. J. Phys. France 1964;25:507-515.

[36] Krimmel A, Mutka H, Koza M M, Tsurkan V, Loidl A. Spin excitations in frustrated A-site spinels investigated with inelastic neutron scattering. Phys. Rev. B. 2009;79:134406.

[37] Fichtl R, Tsurkan V, Lunkenheimer P, Hemberger J, Fritsch V, Krug von Nidda H-A, Scheidt E-W, Loidl A. Orbital freezing and orbital glass state in $FeCr_2S_4$. Phys. Rev. Lett. 2005;94:027601.

[38] Fritsch V, Hemberger J, Büttgen N, Scheidt E W, Krug von Nidda H A, Loidl A, Tsurkan V. Spin and

Orbital Frustration in $MnSc_2S_4$ and $FeSc_2S_4$. Phys. Rev. Lett. 2004;92:116401.

[39] Bergman D, Alicea J, Gull E, Trebst S, Balents L. Order-by-disorder and spiral spin-liquid in frustrated diamond-lattice antiferromagnets. Nature Phys. 2007;3:487-491.

[40] Chen G, Balents L, Schnyder A P. Spin-Orbital Singlet and Quantum Critical Point on the Diamond Lattice: $FeSc_2S_4$. Phys. Rev. Lett. 2009;102:096406.

[41] Goodenough J B, Loeb A L. Theory of Ionic Ordering, Crystal Distortion, and Magnetic Exchange Due to Covalent Forces in Spinels. Phys. Rev. 1955;98:391-408.

[42] J. Kanamori. Superexchange interaction and symmetry properties of electron orbitals. J. Phys. Chem. Sol. 1959;10:87-98.

[43] Wilkinson M K, Cable J W, Wollan E O, Koehler W C. Neutron Diffraction Investigations of the Magnetic Ordering in $FeBr_2$, $CoBr_2$, $FeCl_2$, and $CoCl_2$. Phys. Rev. 1959;113:497-507.

[44] Gingras M J, Stager C V, Raju N P, Gaulin B D, Greedan J E. Static Critical Behavior of the Spin-Freezing Transition in the Geometrically Frustrated Pyrochlore Antiferromagnet $Y_2Mo_2O_7$. Phys. Rev. Lett. 1997;78:947-950.

[45] Fukushima J, Hayashi Y, Takizawa H. Structure and magnetic properties of $FeAl_2O_4$ synthesized by microwave magnetic field irradiation. J. Asian Ceram. Soc. 2013;1:41-45.

[46] Mukhtar F, Kayani Z N, Riaz S, Naseem S. Effect of in-situ oxidation on structure and ferromagnetic properties of Fe_3Al and $FeAl_2O_4$ thin films prepared by electrodeposition. Ceram. Int. 2018;44:9550-

9560.

[47] Yaseen M, Mahmood Q, Ramay S M, Ali I, Naz M Y, Mahmood A. The First-Principle Study of the Electronic Structure, Ferromagnetic and Thermoelectric Properties of Spinel Alloy $FeAl_2O_4$ Using mBJ Functional Approach. J. Supercond. Nov. Mag. 2018;31:1435-1441.

[48] Verwey E J W. Electronic Conduction of Magnetite (Fe_3O_4) and its Transition Point at Low Temperatures. Nature 1939;144:327-328.

[49] Verwey E J W, Haaymann P W. Electronic conductivity and transition point of magnetite ("Fe_3O_4"). Physica. 1941;8:979-987.

Table 1 Experimental results of product $FeAl_2O_4$ samples with respect to the refined structure and magnetic characteristics

	1200_200	1200_40	1200_0	1100_36	1100_0	900_36	900_28
***a* (Å)**	8.15958(1)	8.16070(2)	8.15999(1)	8.16285(2)	8.16151(1)	8.16253(3)	8.16376(6)
u	0.26399(4)	0.26377(6)	0.26387(4)	0.26381(5)	0.26354(4)	0.26382(5)	0.26375(7)
y	0.1220(14)	0.1348(16)	0.1606(12)	0.1358(14)	0.1726(10)	0.1578(14)	0.1710(20)
R_{wp}	4.160	4.016	3.118	2.816	2.500	2.907	3.508
S	2.893	2.636	2.011	1.768	1.585	1.839	2.21
C_{mol} **(emu K/Oe)**	3.80	3.93	3.85	3.90	3.92	4.47	7.07
p_{eff}	5.51	5.60	5.54	5.55	5.59	5.96	7.53
g	2.25	2.29	2.26	2.28	2.28	2.44	3.07
Θ **(K)**	-124.5	-128.9	-132.1	-134.0	-138.9	-164.8	-265.1
T_g **(K)**	11.4	12.5	12.2	13.2	13.4	15.2	39.5

Figure captions

Figure 1 (a) XRD patterns of product $FeAl_2O_4$ samples. (b) SXRD patterns pf 900_28.

Figure 2 Relationship between the inversion parameter and the lattice constant of product $FeAl_2O_4$ samples. The plotted color of each sample corresponds to that in Figure 1. The square symbol (■) indicates the quenched sample. The other symbols indicate the rate of cooling as a circle (● : 25 ºC/h), an inverted triangle (▼ : 19.4 ºC/h) and a triangle (▲ : 5 ºC/h) , respectively.

Figure 3 FT-IR spectra normalized by the highest peak in the band around 675 cm^{-1} of product $FeAl_2O_4$ samples. The plotted color of each sample corresponds to that in Figure 1.

Figure 4 Temperature dependence of the reciprocal χ_{DC} measured for 1200_200 as a typical $1/\chi_{DC}$-T curve of product $FeAl_2O_4$ samples. The insert shows the frequency dependence of the χ_{AC}-T curve of the same sample.

Figure 5 Calculated g values of product $FeAl_2O_4$ samples plotted against the inversion parameter. The plotted color of each sample corresponds to that in Figure 1. Plotted symbols are distinguished by the cooling speed of the sample as a square (■: quenched), a circle (●: 25 ºC/h), an inverted triangle (▼: 19.4 ºC/h) and a triangle (▲: 5 ºC/h), respectively.

Figure 6 Relationship between the inversion parameter and the cusp temperature, T_g, (filled symbols plotted on the left y-axis scale) and the absolute values of the Weiss temperature, $|\Theta|$, (cross mark, ×, plotted on the right y-axis scale) of product $FeAl_2O_4$

samples. Plotted symbols of T_g are distinguished by the cooling speed of the sample as a square (■: quenched), a circle (●: 25 °C/h), a inverted triangle (▼: 19.4 °C/h) and a triangle (▲: 5 °C/h), respectively. The plotted color of each sample corresponds to that in Figure 1.

Figure 7 Dependence of the DC susceptibility at 10 kOe on the temperature for the zero field cooled measurement. The data are plotted for 1200_200 (brown circle) and 900_28 (green circle). The insert shows the field dependence of the χ_{DC}-T curve for 900_28.

Figure 8 Deatil of SXRD peaks of some $FeAl_2O_4$ samples in this study. The plotted color of each sample corresponds to that in Figure 1.